R. & M. No. 3096
(16,107)
A.R.C. Technical Report

MINISTRY OF SUPPLY

AERONAUTICAL RESEARCH COUNCIL
REPORTS AND MEMORANDA

An Analysis of Steady Straight Flight with Inclined Thrust

By

S. B. GATES and A. W. THORPE

LONDON: HER MAJESTY'S STATIONERY OFFICE
1959
PRICE 11s. 6d. NET

An Analysis of Steady Straight Flight with Inclined Thrust

By

S. B. GATES and A. W. THORPE

COMMUNICATED BY THE DIRECTOR-GENERAL OF SCIENTIFIC RESEARCH (AIR), MINISTRY OF SUPPLY

Reports and Memoranda No. 3096*

March, 1953

Summary.—Griffith's proposal to achieve vertical take-off and landing at the usual attitude demands sea-level thrust considerably greater than the weight and continuously rotatable through 90 deg. A study of the steady states of such a system is necessary as a preliminary to work on the flying techniques involved in the project. In this survey a vectorial method of analysis has proved useful in displaying the special features of the performance of such aircraft at both high and low speed.

The main conclusions are:

(*a*) The high-speed performance is sensibly a maximum when the thrust is along the axis of minimum drag. Hence inclining the thrust is useless except in the grounding operations.

(*b*) When the thrust exceeds the weight by a substantial margin, steady flight is confined to very high speed in a very small incidence range. In this regime there are two flight-path angles for every incidence.

(*c*) Handling may therefore be difficult until, with increase of height, the thrust has fallen below the weight. If this proves to be so, it is suggested that the full thrust should be used to climb out of the 'excess thrust' region as quickly as possibly. The aerodynamic dividends in increased height and speed of economic cruise are obvious, but no attempt is made at a project assessment.

(*d*) At very low speed, the attitude corresponding to any given inclination of the thrust is almost constant, and a large range of low speeds and flight-path angles is possible.

1. *Introduction.*—Griffith has proposed that in jet aircraft for which the sea-level thrust can be made to exceed the weight, the thrust should be continuously rotatable through 90 deg from its normal direction, in order that the aircraft should take off and land vertically in the usual attitude. This introduces two novel features into the calculation of steady performance, for the thrust/weight ratio demanded is well outside our present experience and the thrust angle provides a new degree of freedom. It may be useful, therefore, to see what the extended performance field looks like in broad outline. An analysis based on the simplest assumptions† is given below, with some numerical examples.

* R.A.E. Report Aero. 2490, received 28th August, 1953.

† We have neglected

(*a*) the variation of thrust with forward speed

(*b*) the interference of the inclined jet on the aerodynamics of the system without thrust

(*c*) the effect of variable air density in non-level flight.

2. *Analysis.*—The aircraft is in equilibrium, as shown in Fig. 1, under three forces:

Weight W,

Thrust λW inclined at β upwards to chord,

Resultant aerodynamic force R inclined at θ_0 forward of the upward normal to the chord.

The chord is inclined at θ to the horizontal, the incidence is α, and γ is the angle of climb.

It seems convenient in this analysis to work directly from the triangle of forces (Fig. 2), instead of resolving them in the usual way. In Fig. 2 we introduce $\varepsilon = \frac{1}{2}\pi - \beta - \theta$, the inclination of the thrust to the vertical.

The triangle of forces then gives

$$\frac{R}{\sin \varepsilon} = \frac{W}{\cos (\beta + \theta_0)} = \frac{\lambda W}{\cos (\beta + \theta_0 + \varepsilon)},$$

from which it follows that

$$\lambda \cos (\beta + \theta_0) = \cos (\beta + \theta_0 + \varepsilon) \quad .. \quad .. \quad .. \quad .. \quad .. \quad (1)$$

and

$$\frac{R}{W} = \frac{C_R}{w} q = \sqrt{(\lambda^2 - 2\lambda \cos \varepsilon + 1)}, \quad .. \quad .. \quad .. \quad (2)$$

where C_R is the resultant aerodynamic force coefficient, w the wing loading, and q the dynamic pressure.

All the possible attitudes of the aircraft are obtained through equation (1), which gives ε when λ, β, θ_0 are specified, and then the attitude θ follows from

$$\theta = \tfrac{1}{2}\pi - \beta - \varepsilon. \quad .. \quad .. \quad .. \quad .. \quad .. \quad .. \quad (3)$$

The incidence and speed are obtained by means of equation (2) when the aerodynamics of the system is specified. In general C_R and θ_0 are functions of incidence and Mach number:

$$C_R = f_1(\alpha, M) \quad .. \quad .. \quad .. \quad .. \quad .. \quad .. \quad .. \quad (4)$$

$$\theta_0 = f_2(\alpha, M). \quad .. \quad .. \quad .. \quad .. \quad .. \quad .. \quad (5)$$

Since q is proportional to M^2 at a given altitude, equations (2), (4) and (5) suffice to determine C_R, α and M. The angle of climb is then given by

$$\gamma = \theta - \alpha. \quad .. \quad .. \quad .. \quad .. \quad .. \quad .. \quad (6)$$

When compressibility can be neglected the analysis is much simpler, for then (removing M from equations (4) and (5)), α and C_R follow directly from θ_0, and the indicated speed is then given by (2). This applies, of course, to the low-speed performance, which is of particular interest in this project.

3. *Aerodynamic Data.*—In this analysis we describe the aerodynamics in terms of C_R and θ_0* instead of C_L and C_D. Making the usual assumptions about the latter for incidences well below the stall:

$$C_L = a\alpha$$

$$C_D = C_{D0} + kC_L^2 = C_{D0} + ka^2\alpha^2 ,$$

where a, C_{D0}, and k are functions of M.

We then have

$$C_R^2 = C_L^2 + C_D^2$$

$$= C_{D0}^2 + a^2(1 + 2kC_{D0})\alpha^2 + k^2a^4\alpha^2 \quad .. \quad .. \quad .. \quad (4a)$$

and

$$\tan(\alpha - \theta_0) = \frac{C_D}{C_L}$$

$$= \frac{C_{D0}}{a\alpha} + ka\alpha . \quad .. \quad .. \quad .. \quad .. \quad .. \quad .. \quad (5a)$$

Illustrative values of a, C_{D0}, and k are plotted against M in Fig. 3. These have been estimated for a delta aircraft having leading-edge sweep of about 50 deg and 10 per cent thickness/chord ratio.

C_R and θ_0 are shown as functions of α, M in Figs. 4 and 5 and the complete curves of C_R and θ_0 at $M = 0$ are sketched in Fig. 6 up to an incidence of 90 deg. The model data cease at $\alpha = 30$ when θ_0 is zero and we know nothing of the characteristics of this plan-form in the remainder of the range. Tests of early aircraft models with straight wings show that the subsequent variation of θ_0 is small and that C_R rises slowly. The broken parts of the curves are guessed.

Although it is not used in this analysis it may be useful to keep track of the drag/lift ratio C_D/C_L. If γ_0 is the angle of climb at zero thrust we have

$$-\gamma_0 = \tan^{-1}\frac{C_D}{C_L} = \alpha - \theta_0 ,$$

and maximum efficiency occurs at the incidence for which γ_0 is a maximum.

γ_0 is plotted against α for low Mach number in Fig. 7. Its values at large M can be seen from the θ_0 plot in Fig. 4 if the oblique axis OK is used instead of the horizontal axis. Its maximum occurs at about $\alpha = 5$ deg for low M (Fig. 7) and at rather larger incidences in the compressible region (Fig. 4).

The analysis has to take account of negative incidence, which, as we shall see, monopolises most of the performance diagram at high speed when the thrust exceeds the weight. We assume

* The angle θ_0 has been used in spite of its awkward numerical values because it is traditional and is the attitude for zero thrust.

that the aircraft is aerodynamically symmetrical about the chord. Then if the resultant force is at θ_0 to the upward normal to the chord when the incidence is α, it will be at θ_0 to the downward normal when the incidence is $-\alpha$, and its angle referred to the upward normal is $\pi - \theta_0$. Thus if equation (1) refers to α, the equation for $-\alpha$ is obtained by substituting $\pi - \theta_0$ for θ_0 :

$$\lambda \cos(\beta - \theta_0) = \cos(\beta - \theta_0 + \varepsilon). \quad .. \quad .. \quad .. \quad .. \quad .. \quad (1a)$$

With these conventions the minimum value of θ_0 is by definition -90 deg, corresponding to $\alpha = 0$. Its maximum is small and positive, about 5 deg in the case illustrated. The thrust angle β is taken to vary from 0 to 90 deg.

4. *Graphical Solution for Attitude.*—There is a simple graphical construction which is useful in sorting out the various attitudes θ given by the above equations. The principle of this construction is shown in Fig. 8. Starting with the vertical weight vector AO, we allow the thrust vector λW (represented by OP) to describe a circle. PA then represents the aerodynamic force vector and AOP is the triangle of forces. If now we fix the thrust angle β we can insert at P the right angle CPN representing the aircraft, PC being the chord and PN the upward drawn normal. This determines the angles θ and θ_0 as shown. The construction shown at P is for a positive incidence. A similar construction for negative incidence (in which θ_0 must be referred to the downward drawn normal) is shown at Q, and is distinguished by drawing the aircraft CQN with broken lines. Three of these circular constructions are drawn, in order to show how the diagram changes in type according as λ is less than, equal to, or greater than 1.

Starting with fixed values of λ and β we can construct all the solutions for positive incidence by following the point P round the circle, and all those for negative incidence by following the point Q, rejecting, however, those that are aerodynamically inadmissable, that is, those for which θ_0 is less than -90 deg or greater than some small positive angle depending on the design being considered, in this case about 5 deg.

We can also reject on practical grounds the inverted attitudes, those in which the upward normal to the chord is below the horizontal. If this is done, the range of attitude for a given λ, as β varies from 0 to 90 deg, can be usefully displayed on a few sectorial diagrams. These have been drawn for $\lambda = 0{\cdot}75$, 1 and $1{\cdot}5$ in Figs. 8, 9 and 10 respectively. A few notes on these may be useful:

$\lambda = 0{\cdot}75$ (Fig. 9).—The sectors are bounded below by the onset of the inverted range at negative incidence, and above by the aerodynamic limit $\theta_0 = 5$ deg at positive incidence. The solution for positive and negative incidences meet at $\theta_0 = -90$, where α must be zero. The whole aerodynamic range for positive α is always available ; that for negative α is limited by the exclusion of inverted attitudes.

$\lambda = 1{\cdot}0$ (Fig. 10).—The same remarks apply to the lower limit of the sector, but its upper limit is always at the zenith A, which represents of course the stationary condition. The attitude at A is 90 deg $- \beta$ and the value of θ_0, regarded as the limit from positions to the left of A, is $-\beta$. There is a discontinuity in the vector diagram at A, for as we pass through it in the clockwise sense the direction of R jumps through 180 deg and solutions to the right of A are inadmissable. Thus the aerodynamic range for positive incidence is limited to that between $\theta_0 = -90$ and $\theta_0 = -\beta$. It narrows as β increases and vanishes at $\beta = 90$, where only negative incidence is possible.

$\lambda = 1{\cdot}5$ (Fig. 11).—When λ exceeds unity, the point A lies inside the circle, and the general mechanics of the system reduces the aerodynamic range (represented by θ_0) which could otherwise be used.

It is clear from equations (1) and (1*a*) that when $\lambda > 1$ we must have

$$|\cos(\beta + \theta_0)| < 1/\lambda \text{ when } \alpha > 0$$

and

$$|\cos(\beta - \theta_0)| < 1/\lambda \text{ when } \alpha < 0 .$$

These conditions are connected with the geometry of Fig. 8, from which it easily follows that the maximum angle subtended at the circumference by AO is δ, where $\sin \delta = 1/\lambda$.

It is shown in Appendix II that the conditions may be written

$$-\delta < \beta + \tfrac{1}{2}\pi + \theta_0 < \delta , \quad \alpha > 0$$

and

$$-\delta < \beta - \tfrac{1}{2}\pi - \theta_0 < \delta , \quad \alpha < 0$$

or

$$\left.\begin{aligned} -\delta - \beta - \tfrac{1}{2}\pi < \theta_0 < \delta - \beta - \tfrac{1}{2}\pi , \quad \alpha > 0 \\ -\delta + \beta - \tfrac{1}{2}\pi < \theta_0 < \delta + \beta - \tfrac{1}{2}\pi , \quad \alpha < 0 \end{aligned}\right\} \quad \ldots \quad \ldots \quad \ldots \quad (7)$$

The inequalities (7) give the maxima and minima of θ_0 when λ and β are given.

In the case illustrated ($\delta = 41{\cdot}8$) these limits are:

	$\alpha > 0$		$\alpha < 0$	
β	$\theta_{0\max}$	$\theta_{0\min}$	$\theta_{0\max}$	$\theta_{0\min}$
0	−48·2	−131·8	−48·2	−131·8
20	−68·2	−151·8	−28·2	−111·8
40	−88·2	−171·8	−8·2	−91·8
41·8	−90		−6·6	−90
60			+11·8	−71·8
80			31·8	−51·8
90			+51·8	−31·8

The solutions for positive incidence have $\theta_{0\max}$ at B and $\theta_{0\min}$ at C ; and *vice versa* for negative incidence.

With these figures in mind we can turn to the rather complex diagrams of Fig. 11:

At $\beta = 0$, θ_0 for positive α decreases on each side of B from −48·2 at B to −131·8 at C. The aerodynamic limit −90 occurs at the zenith and the nadir. The solutions for negative α are the reflection of these, starting from C ; they are all inverted. The practical sector is therefore the left-hand semi-circle.

At $\beta = 20$, θ_0 for positive α decreases from −68·2 at B to −90 at D and E. θ_0 for negative α decreases from −28·2 at C to join the positive solutions at D and E. The practical sector is the semi-circle stopped by the inversion limits at F and G.

As β increases this process continues with the positive-incidence sector DE decreasing about B (*see* $\beta = 40$), until at $\beta = 41{\cdot}8$ (not shown) it has shrunk to nothing. At this value of β the negative-incidence solutions decrease from $-6{\cdot}6$ at C to -90 at B. The practical semi-circle, limited by inversion, consists entirely of negative-incidence solutions.

At $\beta = 60$, the negative-incidence solutions are $\theta_0 = 11{\cdot}8$ at C and $-71{\cdot}8$ at B. The practical sector FG is now less than a semi-circle, F being determined by the aerodynamic limit $\theta_0 = 5$ and G by inversion. The diagram for $\beta = 90$ follows the same pattern.

5. *Features of Steady Flight with Thrust Exceeding Weight.*—Two important aerodynamic onclusions follow from the above discussion of the possible values of θ_0 when $\lambda > 1$:

The first is that only a very small range of positive incidence can be used. The maximum value of θ_0 for positive incidence occurs when $\beta = 0$ and is $-\cos^{-1}(1/\lambda)$, which decreases as λ increases. In the example illustrated ($\lambda = 1{\cdot}5$) its value is $-48{\cdot}6$. Thus when $\beta = 0$ the whole of the flight range between vertical ascent and vertical descent is accomplished with values of θ_0 between -90 and $-48{\cdot}6$ (Fig. 11). The plot of θ_0 in Fig. 4 shows that in incompressible flow the maximum usable incidence would be less than $0{\cdot}2$ deg, and when, as it must be, the variation with M is considered, the value is still no more than about half a degree. As we have seen above, this range decreases with increase of β, and vanishes when $\beta = 41{\cdot}8$.

The second point is that there are always two possible attitudes at a given θ_0, whether the incidence is positive or negative. When the speed is slow enough for compressibility to be neglected, so that θ_0 fixes α and α fixes the control angle, this suggests that there are always two attitudes for a given control angle. At high speed it will still be true that there are two attitudes for a given incidence, but their difference in speed will in general require different control angles.

There is clearly here a handling problem that should be looked into.

6. *Performance Diagrams.*—Before discussing some performance diagrams we may remind ourselves of the essential features of the aerodynamic data, since it is these that govern the general shape of the diagrams. The most remarkable of these is the shape of the θ_0 curve (Fig. 6), which shows that in incompressible flow θ_0 increases very rapidly from -90 deg to 0 deg in a few degrees of incidence, rises slowly to a small positive maximum below the stall and thereafter decreases very slowly, possibly to a small negative minimum, before reaching zero at $\alpha = 90$. In short, the resultant-force vector, starting from coincidence with the reversed chord at zero incidence, sweeps rapidly into position with the normal and remains near it, while its amplitude increases at first rapidly and then, after the stall, at a decreasing rate.

In a broad survey of this sort the performance is best displayed in a series of vector diagrams of forward speed, at fixed values of β, arranged so that the corresponding attitudes can be visualised. The variation of θ_0 suggests that the survey can be divided into two parts at an incidence of about 10 deg:

(*a*) High-speed range, $0 < \alpha < 10$, where the aerodynamic variation with M (Figs. 4, 5) must be used. In this range the variation of α is small and that of θ_0 is large. The results depend on altitude, and are computed mainly for sea level.

(*b*) Low-speed range, $10 < \alpha < 90$, where the variation of θ_0 is small and that of α is large. The flow is incompressible and these results apply to all altitudes, indicated speed being used.

Three values of λ ($0{\cdot}75$, $1{\cdot}0$, $1{\cdot}5$) are considered, with a wing loading of 50. The largest value of λ is rather more than the minimum (about $1{\cdot}3$) estimated to be necessary for the grounding operation.

6.1. *Low-Speed Range.*—Since the small variation in θ_0 is uncertain, and is minor in its effect, we can get a good approximate picture of the regime by using $\theta_0 = 0$. Sector diagrams showing the admissible attitudes and their relation to β are drawn in Fig. 12. At $\lambda = 0{\cdot}75$, θ is always positive, ranging from 0 to $\sin^{-1}\lambda = 49{\cdot}6$, while β ranges from 90 to 0; the incidence is always positive. At $\lambda = 1{\cdot}5$, θ is again always positive, ranging from 0 to 90, while β ranges from 90 to $\cos^{-1}(1/\lambda) = 48{\cdot}2$; the incidence is always negative. At $\lambda = 1$, on the other hand, the only possible solutions are inverted ones at negative incidence. At $\lambda = 1$ we are left, therefore, only with the stationary position, where θ_0 becomes meaningless; these are given by $\theta = 90° - \beta$.

So much for the geometry. Analytically θ is given as a function of β by equations (1) and (3). Thus at given β the attitude is fixed, and the vector diagram of V_i can be constructed on the chord as datum after calculating V_i as a function of α from equation (2), using C_R from Fig. 6.

The vector diagrams for $\lambda = 0{\cdot}75$ and $1{\cdot}5$ are shown in Figs. 13 and 14. To interpret these it is only necessary to observe, for example, that at $\lambda = 0{\cdot}75$, $\beta = 0$ (the first diagram of Fig. 13), the attitude is fixed at $\theta = 49{\cdot}6$ as shown, and the aircraft can move along any of the arrows shown with velocity proportional to its length. It may be observed, too, from a survey of the whole Figure that the bounding curve of the velocity vectors rotates with the chord as β increases, retaining its shape but shrinking in linear dimensions by a factor proportional to $(\lambda^2 - 2\lambda\cos\varepsilon + 1)^{1/4}$ (*see* equation 2).

The trivial stationary solutions for $\lambda = 1$ are shown in Fig. 15 to round off the series.

These diagrams are only intended to give a rough idea of the flight positions which will be possible when an aircraft is equipped with inclined thrust, jet controls and automatic stabilisers in order to take off and land vertically with jet lift. As this project proceeds we shall have to study the motions of transition between the jet-borne and the air-borne states in the process of working out a flying technique. Some at least of the solutions shown may not turn out to be so academic as they seem at first sight. For example, the diagrams for $\beta = 90$ at both values of λ are of direct interest, one representing the ascending regime with $\lambda > 1$ and the other the descending regime with $\lambda < 1$.

6.2. *High-Speed Range.*—A method of computation for constructing a vector diagram of high-speed performance from the analysis of Section 2 is given in Appendix I. The results for $\lambda = 0{\cdot}75$, $1{\cdot}0$, $1{\cdot}5$; $w = 50$, at sea level are given in Figs. 16 to 18. In these diagrams the incidence never exceeds 5 deg and is for the most part much smaller; the curves are broken off where necessary (Figs. 16 and 18) to exclude the low-speed region near the origin, for which an approximation has already been discussed. As the incidence is small, the attitude is well enough defined by the direction of the speed vector. Any curve at constant β is shown by a full line when the incidence is positive and by a broken line when the incidence is negative. The incidence is marked in degrees on a few of the curves.

The families of vectorial curves shown in the diagrams, though they differ widely in shape and in variation with the parameter β, have these features in common, that they never intersect and they approach the origin as β increases from 0 to 90 in such a way that the speed vector at any given γ continually decreases.

In short the performance appears from the computations to be a maximum at or near $\beta = 0$. The question of maximum performance is discussed in detail in Appendix III. It is shown

there that although the maximum performance does not occur exactly at $\beta = 0$, the maximum-performance curve is so near to $\beta = 0$ that we may treat it as giving the maximum for all practical purposes.

It was necessary to explore the performance variation with β in as much detail as is shown in these diagrams in order to sketch a pioneer map of the subject. They show however that inclined thrust is practically useless in the high-speed range, and that we may concentrate on $\beta = 0$, the three curves for which are drawn together in Fig. 19. If, for example, we are provided with $\lambda = 1{\cdot}5$ and wish to fly at less than maximum performance it is clearly more economical to reduce the thrust at $\beta = 0$ (Fig. 19), than to increase β at maximum thrust (Fig. 18).

There are some essential differences between flight at $\lambda < 1$ and flight at $\lambda > 1$*, which are seen by comparing Figs. 16 and 18, or more summarily in Fig. 19 for $\beta = 0$. Consider, for instance, the curve for $\lambda = 0{\cdot}75$ and $1{\cdot}5$ in Fig. 19. At $\lambda = 1{\cdot}5$ the incidence starting at zero in the vertical dive increases continually along the performance curve, and would continue to do so beyond the point $\alpha = 4{\cdot}0$ at which the curve is arbitrarily broken off. The whole range of incidence can be used, though only a very small range (0 to $0{\cdot}7$ deg) occurs between dive and maximum rate of climb. In contrast, at $\lambda = 1{\cdot}5$ the incidence is zero at vertical dive and vertical climb and reaches a very small maximum, about $0{\cdot}45$ deg, between them. Thus the whole of steady flight is confined to an incidence range of about half a degree, and at every value in this range there are two positions of equilibrium. This exemplifies a principle, already stated in Section 5, which can be traced in detail as β increases in Figs. 16 and 18. At $\lambda = 0{\cdot}75$ each β curve is monotonic in α and positive incidence occupies most of the diagram. At $\lambda = 1{\cdot}5$ each value of α occurs twice on a β curve and most of the diagram is occupied by negative incidence.

The diagram for $\lambda = 1$ separates the regimes discussed above. All the β curves now start from the origin, the stationary position, where the limiting value of θ_0 as the curves run in at small forward speed is $-\beta$. The limiting incidence at the origin as β varies is therefore obtained from the steep part of the θ_0 curve of Fig. 6; it varies from 0 at $\beta = 90$ to $3{\cdot}7$ deg at $\beta = 0$. Positive values of θ_0 are inadmissible, and the low-speed diagram (where θ_0 is assumed to be zero) degenerates to the stationary position represented by the origin on the high-speed diagram.

In order to summarise clearly the complex incidence distributions discussed above, α has been plotted against γ for $\beta = 0$ in Fig. 20.

Finally, referring to Fig. 19, we may note some practical results of increasing λ from $0{\cdot}75$ to $1{\cdot}5$ at sea level:

		Maximum Rate of Climb				*Level Speed*		
λ	$V_C(f,s)$	γ (deg)	M	α (deg)	Climb ratio	M	α (deg)	Speed ratio
$0{\cdot}75$	535	34	$0{\cdot}866$	$0{\cdot}65$	1	$0{\cdot}988$	$0{\cdot}54$	1
$1{\cdot}0$	780	50	$0{\cdot}930$	$0{\cdot}49$	$1{\cdot}46$	$1{\cdot}02$	$0{\cdot}48$	$1{\cdot}035$
$1{\cdot}5$	1080	90	$0{\cdot}965$	0	$2{\cdot}02$	$1{\cdot}145$	$0{\cdot}38$	$1{\cdot}16$

The important point displayed by these figures is that increasing λ from $0{\cdot}75$ to $1{\cdot}5$ multiplies the rate of climb by $2{\cdot}02$ and the level speed by only $1{\cdot}16$. This shows in a general way how the large excess thrust required for vertical ground operation should be used. We have seen that at $\lambda = 1{\cdot}5$, steady flight is confined to speeds near $M = 1$ and to incidences less than half a degree, there being two flight positions for every incidence in this narrow range. How much

* This Section continues the discussion broached in Section 5.

this may embarrass the pilot remains to be seen. He may, however, escape most of these difficulties by rotating the aircraft through 90 deg and the thrust from $\beta = 90$ to 0 soon after he has risen vertically from the ground. He then climbs, at first vertically and then at decreasing angles, at maximum rate while his thrust decreases. His performance at 30,000 ft, where his thrust ratio has fallen to $0{\cdot}75$, is shown in Fig. 21. Here the regime has regained the same general features as that at $\lambda = 0{\cdot}75$ at sea level, which we know from experience with our highest powered fighters is manageable; in particular the incidence at maximum climb has risen to nearly 2 deg. It will be noticed of course that this is very much below the altitude for economic cruising speed, for the level incidence is still only about 1 deg, while that for maximum γ_0 exceeds 5 deg.

Without pursuing this line of argument into the detail necessary for project analysis, we may summarise its trend as follows. The provision of $\lambda > 1$ at sea level for the grounding operation means that handling will be unusual, and may be difficult, up to a height at which the thrust has fallen well below the weight; with $\lambda = 1{\cdot}5$, this is about 30,000 ft. On the other hand, the pilot has a spectacular rate of climb off the ground at $\beta = 0$ which he can use, in the case examined, to reach his 'safe' height in less than a minute. Thereafter, with the attainment of normal flying conditions, the advantages of very high sea-level thrust begin to accrue in increasing the altitude and speed of economic cruise.

The above discussion applies only to jet thrust, and is not relevant to rocket thrust, whose law of variation with altitude is different.

7. *Conclusions.*

(*a*) The vectorial analysis used in this paper appears to be more convenient than the traditional resolution in the lift and drag directions in displaying the essential features of very high performance, particularly when this is to be combined with jet-borne flight at very low and vanishing speeds.

(*b*) The high-speed performance, as defined by the curve bounding the speed vectors, is sensibly a maximum when the thrust is aligned with the aerodynamic axis of symmetry of the aircraft. Thus, inclining the thrust is useless except to provide vertical take-off and landing in the usual attitude.

(*c*) When the thrust is less than the weight the whole of the incidence range up to the stall and beyond can be used in steady flight. For any incidence there is one steady-flight position. When the thrust is greater than the weight the incidence is zero at vertical climb and vertical dive and rises to a very small maximum in between. For any incidence in this narrow range there are two steady-flight positions. The handling problem in this regime must be investigated.

(*d*) The main advantage accruing to high-speed performance from the large increase of thrust required to achieve jet-borne ground conditions is the increase in rate of climb. In the case examined, doubling the thrust/weight ratio from $0{\cdot}75$ to $1{\cdot}5$ doubles the maximum rate of climb and makes it vertical, while the level speed is increased by less than 20 per cent. In this case, therefore, the tactic would be to 'go up in the lift' until the thrust drops below the weight, and then proceed, under more normal flying conditions, to the optimum height for the operation. The performance, as defined in (*b*), would be increased at every altitude. Its evaluation in terms of cost of the operation is not attempted here.

(*e*) A good approximation to the steady states near the hovering position is got by assuming that the resultant aerodynamic force is normal to the axis of symmetry. At any thrust inclination the attitude is then fixed and the aircraft can move over a range of incidence from about 10 to 90 deg (positive when the thrust is less than the weight, and *vice versa*).

LIST OF SYMBOLS

a		Slope of the lift curve $\partial C_L/\partial\alpha$
C_D		Drag coefficient
C_{D0}		Drag coefficient at zero lift
C_L		Lift coefficient
C_R		Total-force coefficient
k		Induced-drag constant ($C_D = C_{D0} + kC_L^2$)
M		Mach number
p		Atmospheric pressure
p_0		Atmospheric pressure at sea level
q		Dynamic pressure $\frac{1}{2}\rho V^2$
R		Total aerodynamic force
r		Relative pressure p/p_0
V		Aircraft speed
V_i		Indicated aircraft speed
V_x		Horizontal component of aircraft speed
V_z		Vertical component of aircraft speed
w		Wing loading
X	$=$	$\sqrt{\{C_R(q/w)\}}$
α		Angle of incidence
β		Angle between the thrust line and the wing chord
γ		Angle of climb
γ_0		Angle of climb at zero thrust
γ		Ratio of the specific heats for air
δ		Maximum value of the angle between the thrust and the total aerodynamic force for steady flight at $\lambda > 1$
ε		Inclination of the thrust to the vertical
θ		Angle between the chord and the horizontal
θ_0		Angle between the chord and the horizontal at zero thrust (equals angle between the total aerodynamic force and the normal to the chord)
λ		Ratio of thrust to weight
ρ		Air density
φ		Angle between the total aerodynamic force and the chord
	$=$	$\frac{1}{2}\pi + \theta_0$
ψ	$=$	$\alpha + \beta$

APPENDIX I

Method of Calculation of Performance Diagrams

To display the performance characteristics of this type of aeroplane we calculate the velocity vector diagram for constant thrust/weight ratio λ and constant jet-deflection angle β.

We have, from the mechanics of the system, equations (1) and (2) of Section 2

$$\lambda \cos(\beta + \theta_0) = \cos(\beta + \theta_0 + \varepsilon), \quad .. \quad .. \quad .. \quad .. \quad .. \quad (A.1)$$

$$\frac{R}{W} = \frac{C_R}{w} q = \sqrt{(\lambda^2 - 2\lambda \cos \varepsilon + 1)} = X^2 \text{ (say)}. \quad .. \quad (A.2)$$

If we now chose values of θ_0, we may calculate ε from (A.1) and hence X from (A.2). We can also calculate θ from the relation

$$\theta = \tfrac{1}{2}\pi - \beta - \varepsilon. \quad .. \quad .. \quad .. \quad .. \quad .. \quad (A.3)$$

We note that if we are calculating curves for a series of different values of β we shall not require to repeat all these calculations at each β if we chose our interval in θ_0 to be the same as the interval in β. This is because ε and X are functions of $\beta + \theta_0$ only. That is, the direction of the chord is unimportant from the point of view of the mechanics; the important angle is that between the thrust and the aerodynamic force, which is the complement of $\beta + \theta_0$.

Let us now consider the aerodynamic aspect of the problem. We have assumed our data to be given in the form

$$\left.\begin{aligned} a &= a(M) \\ C_{D0} &= C_{D0}(M) \\ k &= k(M) \end{aligned}\right\}. \quad .. \quad .. \quad .. \quad .. \quad .. \quad .. \quad (A.4)$$

These are the coefficients in the expressions for the lift and drag

$$\left.\begin{aligned} C_L &= a\alpha \\ C_D &= C_{D0} + kC_L^2 \end{aligned}\right\}. \quad .. \quad .. \quad .. \quad .. \quad .. \quad (A.5)$$

Hence at any Mach number we can calculate C_L and C_D as functions of α. If the aerodynamic data are given in this form so much the better. From curves of C_L and C_D against α at constant M we can calculate C_R and θ_0 from the relations

$$C_R^2 = C_L^2 + C_D^2, \quad .. \quad .. \quad .. \quad .. \quad .. \quad (A.6)$$

$$\tan(\alpha - \theta_0) = C_D/C_L. \quad .. \quad .. \quad .. \quad .. \quad .. \quad (A.7)$$

From a knowledge of C_R and θ_0 as functions of α we can regard C_R as being a function of θ_0.

Now

$$X = \sqrt{\left(\frac{C_R q}{w}\right)}$$

$$= M\sqrt{\left(\frac{\frac{1}{2}\gamma p C_R}{w}\right)}$$

$$\frac{X}{\sqrt{r}} = M\sqrt{\left(\frac{\frac{1}{2}\gamma p_0 C_R}{w}\right)}. \quad \ldots \quad \ldots \quad \ldots \quad \ldots \quad \ldots \quad \text{(A.8)}$$

Here p is the atmospheric pressure and p_0 its value at sea level ; r is the relative pressure p/p_0 and γ is the ratio of the specific heats for air.

Now C_R is a function of θ_0 at a fixed M and hence if we fix θ_0 we can regard C_R as a function of M only. The right-hand side of equation (A.8) is then dependent on M only and is independent of height. We can therefore plot our aerodynamic data in the form of curves of $X/\sqrt{r}$ against M for constant θ_0. This set of curves can then be used to calculate performance at all heights as follows:

From our calculations of the mechanics we know X as a function of θ_0 and if we have plotted our aerodynamic data for the same values of θ_0 as we use in the calculation of the mechanics, we can by choosing a height (*i.e.*, a relative pressure) calculate $X/\sqrt{r}$ and hence from these curves obtain a value of M without any interpolation between curves.

Since again from the aerodynamics we know θ_0 as a function of α for fixed M, we may plot α against M for fixed θ_0. From these curves we can calculate the incidence.

Knowing M and the height we can calculate the speed V and since we know θ from (A.3) we can calculate the vertical and horizontal components of the speed from the formulae:

$$V_z = V \sin(\theta - \alpha)$$

$$V_x = V \cos(\theta - \alpha).$$

From these data we plot the performance diagram.

APPENDIX II

Angular Relations when $\lambda > 1$

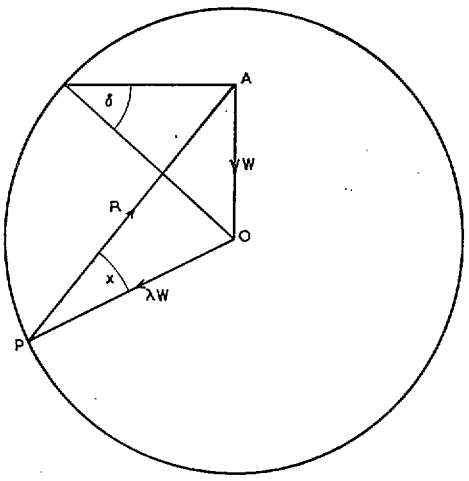

FIG. 1.

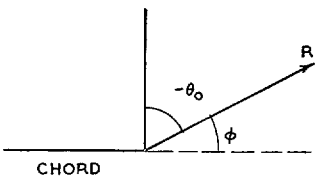

FIG. 2.

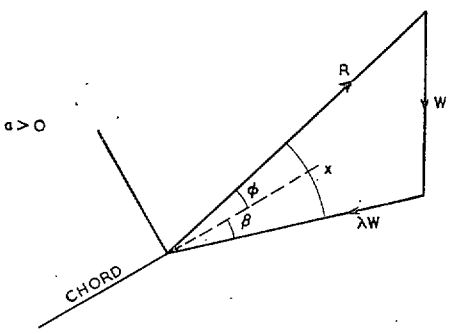

FIG. 3.

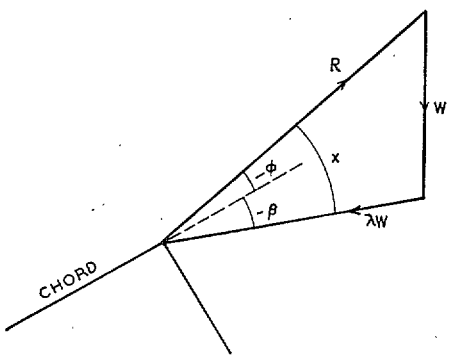

FIG. 4.

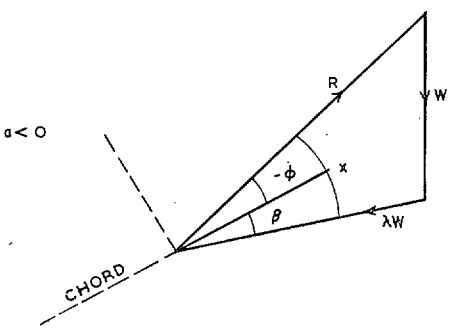

FIG. 5.

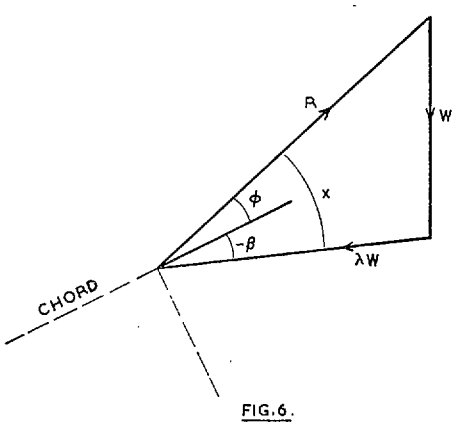

FIG. 6.

Let x be the angle APO between the aerodynamic force and the thrust.

When $\lambda > 1$ we have from the geometry of the circle, $x < \delta$ (Fig. 1). Let ϕ be the inclination of R to the chord reversed (Fig. 2), so that $\phi - \theta_0 = \frac{1}{2}\pi$.

Now let the chord be fixed in relation to the triangle of forces AOP.

There are four cases to consider:

$\alpha > 0$, normal position (Fig. 3), inverted (Fig. 4)

$\alpha < 0$, normal position (Fig. 5), inverted (Fig. 6).

If we start with angles ϕ and β for $\alpha > 0$, normal, these angles are shown in the four cases in Figs. 3, 4, 5 and 6 and we have

$$\begin{aligned} \alpha > 0 \quad x &= \phi + \beta && \text{normal} \\ &= -(\phi + \beta) && \text{inverted} \\ \alpha < 0 \quad x &= \beta - \phi && \text{normal} \\ &= -(\beta - \phi) && \text{inverted.} \end{aligned}$$

The condition $x < \delta$ now gives

$$\begin{aligned} -\delta < \beta + \phi < \delta , \quad \alpha > 0 \\ -\delta < \beta - \phi < \delta , \quad \alpha < 0 , \end{aligned}$$

which are equivalent to those stated in the relation (7) of Section 4.

---

or

$$\tan\psi = 2k\left(\frac{w}{q}\right)(\cos\gamma - \lambda\sin\psi) \quad .. \quad .. \quad .. \quad .. \quad (8)$$

and substituting from (2):

$$\tan\psi = 2kC_L\,. \quad .. \quad .. \quad .. \quad .. \quad .. \quad .. \quad (9)$$

Equation (9) is not strictly an equation which determines ψ because C_L is itself a function of ψ. In order to obtain an equation which determines ψ we should eliminate (w/q) between (8) and (5). This would, however, produce a very complicated equation and we shall see that we can deduce all we need from (9).

For the range of incidence we have considered in the performance diagrams ($C_L < 0{\cdot}3$) we see that $\tan\psi$ will be small for maximum performance.

Now

$$\beta = \psi - \alpha \quad .. \quad .. \quad .. \quad .. \quad .. \quad .. \quad (10)$$

and if ψ is small we may write $\psi = \tan\psi$ so that

$$\beta = 2kC_L - \alpha$$

$$= C_L\left(2k - \frac{1}{a}\right). \quad .. \quad .. \quad .. \quad .. \quad .. \quad (11)$$

On our aerodynamic assumptions $2k - (1/a)$ is a function of Mach number only and at sea level we can find an upper bound for C_L because the lift can not exceed the sum of the weight and the thrust. At low speeds we shall have a further limit on C_L because it must not exceed $C_{L\,\max}$ for the aeroplane. We can find then an upper bound for the value of $|\beta|$ at maximum performance as a function of Mach number. This upper bound is plotted in Fig. 22.

We see that the optimum value of β can not differ from zero by more than a few degrees and only at low speeds can it exceed one degree.

Performance curves have been calculated for $\lambda = 1{\cdot}5$ for $\beta = \pm 1$ deg and within the accuracy of the calculations no difference between the performance was observed. That is the speed did not differ by more than 1 ft/sec at any value of γ.

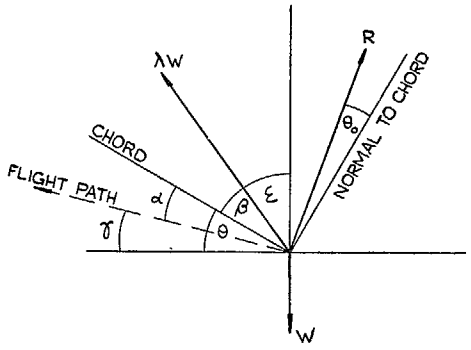

FIG. 1. Forces in equilibrium.

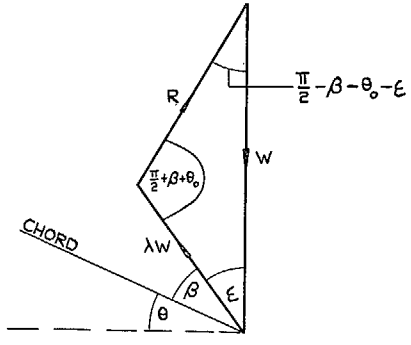

FIG. 2. Triangle of forces.

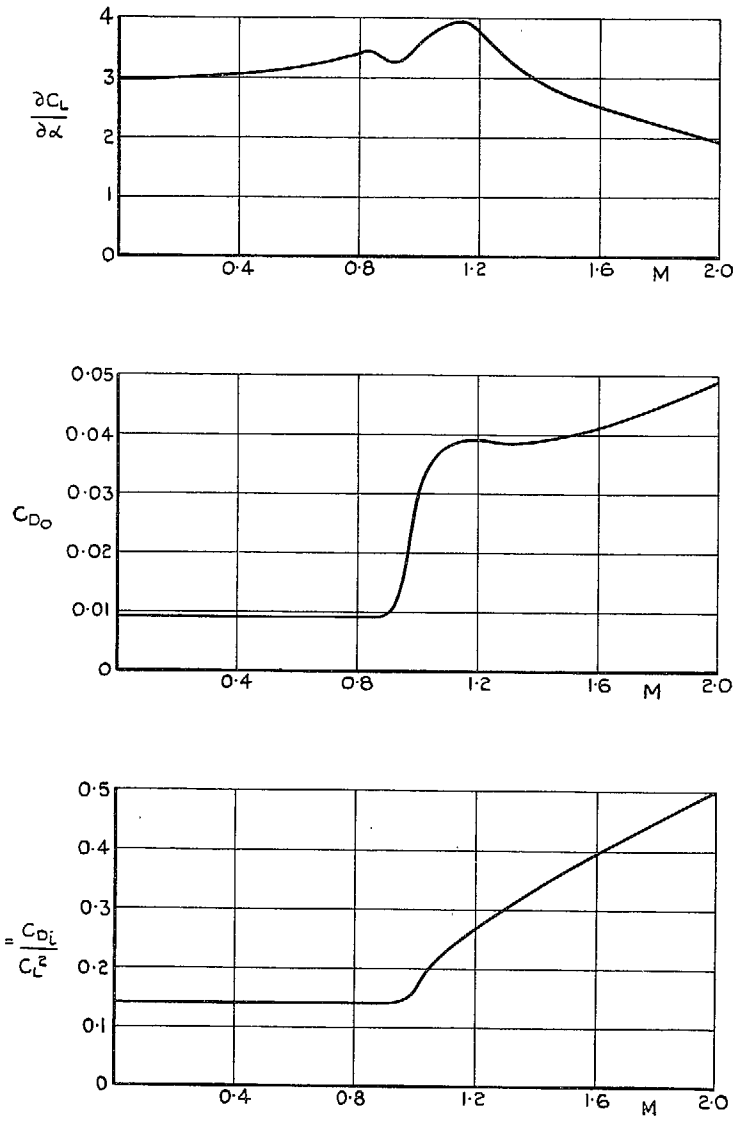

FIG. 3. Variation of lift curve slope, drag coefficient at no lift, and induced-drag factor, with Mach number.

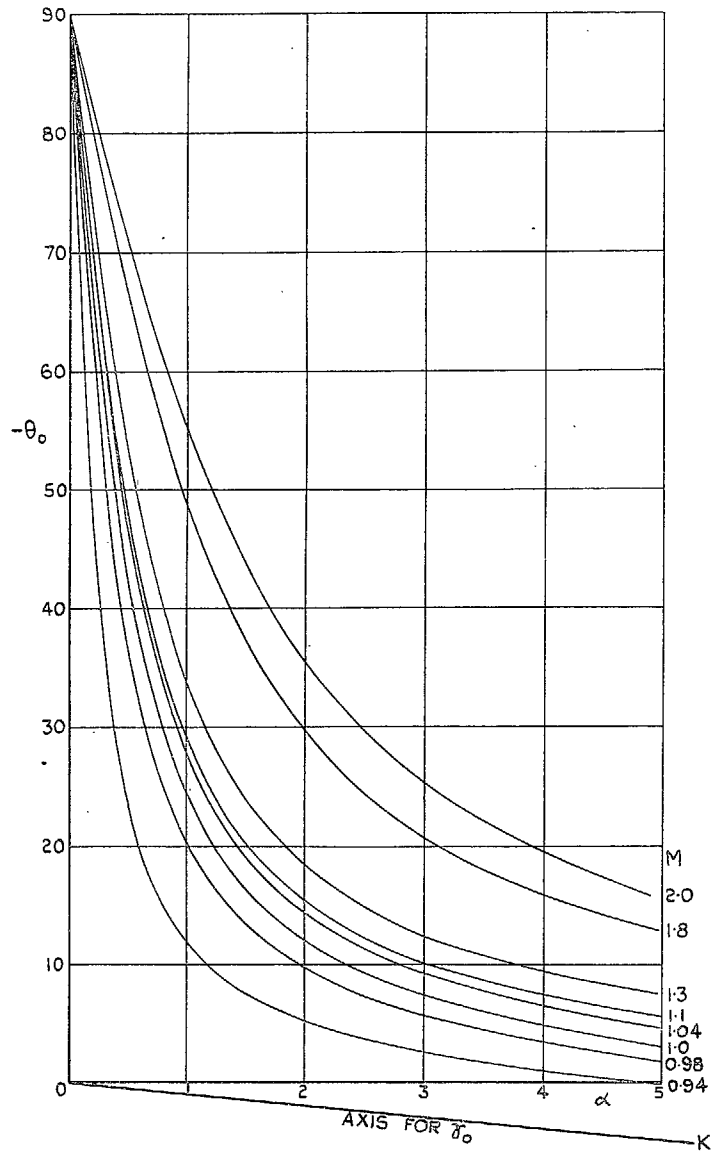

FIG. 4. Variation of θ_0 with incidence at various Mach numbers.

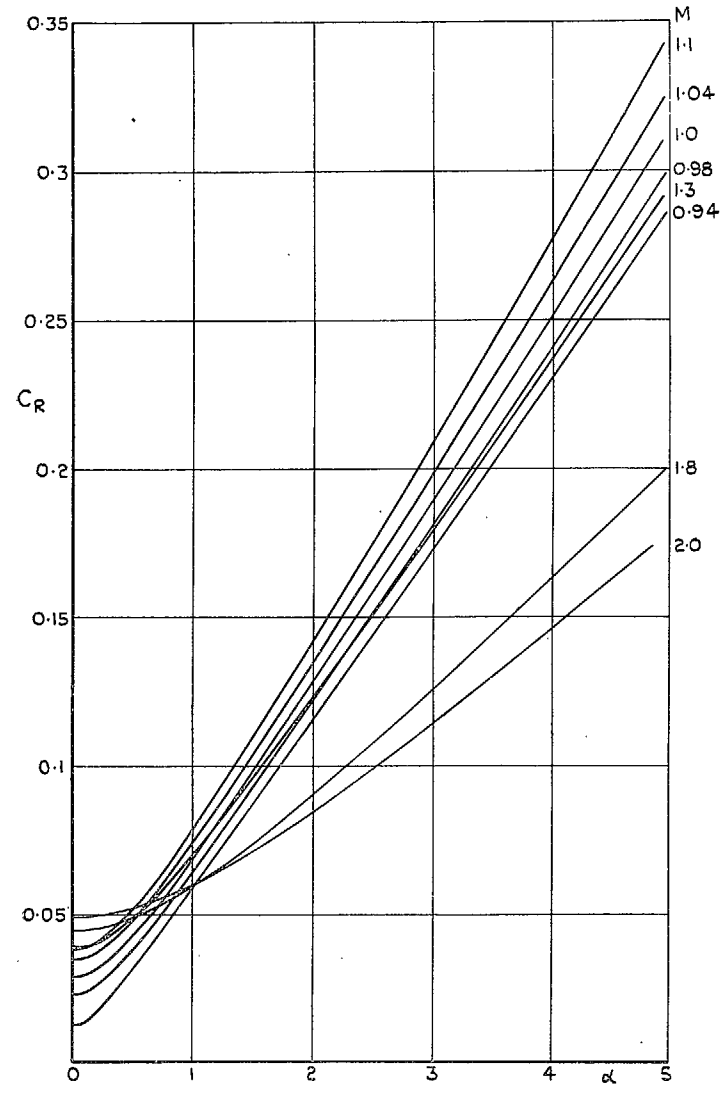

FIG. 5. Variation of C_R with incidence at various Mach numbers.

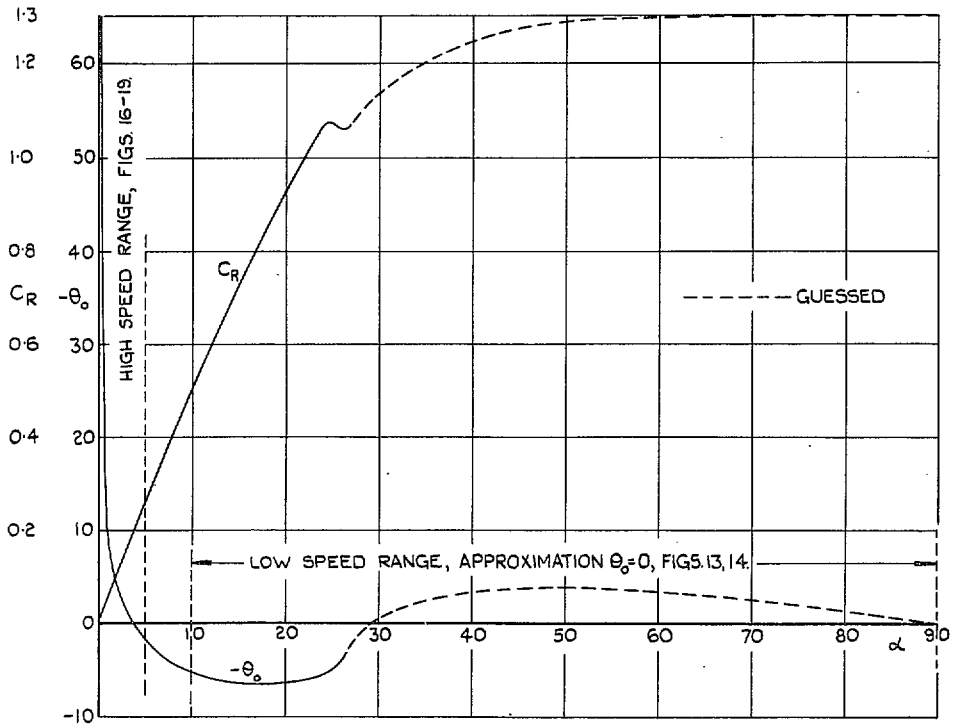

FIG. 6. Variation of C_R and ϑ_0 with incidence at low Mach number.

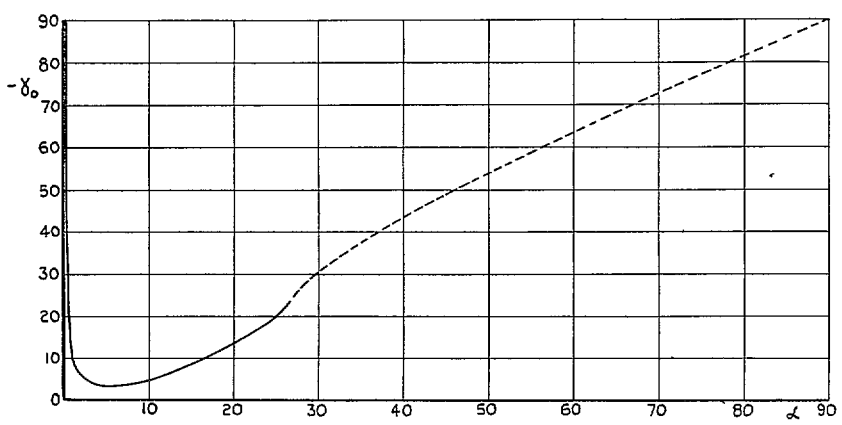

FIG. 7. Variation of γ_0 with incidence at low Mach number.

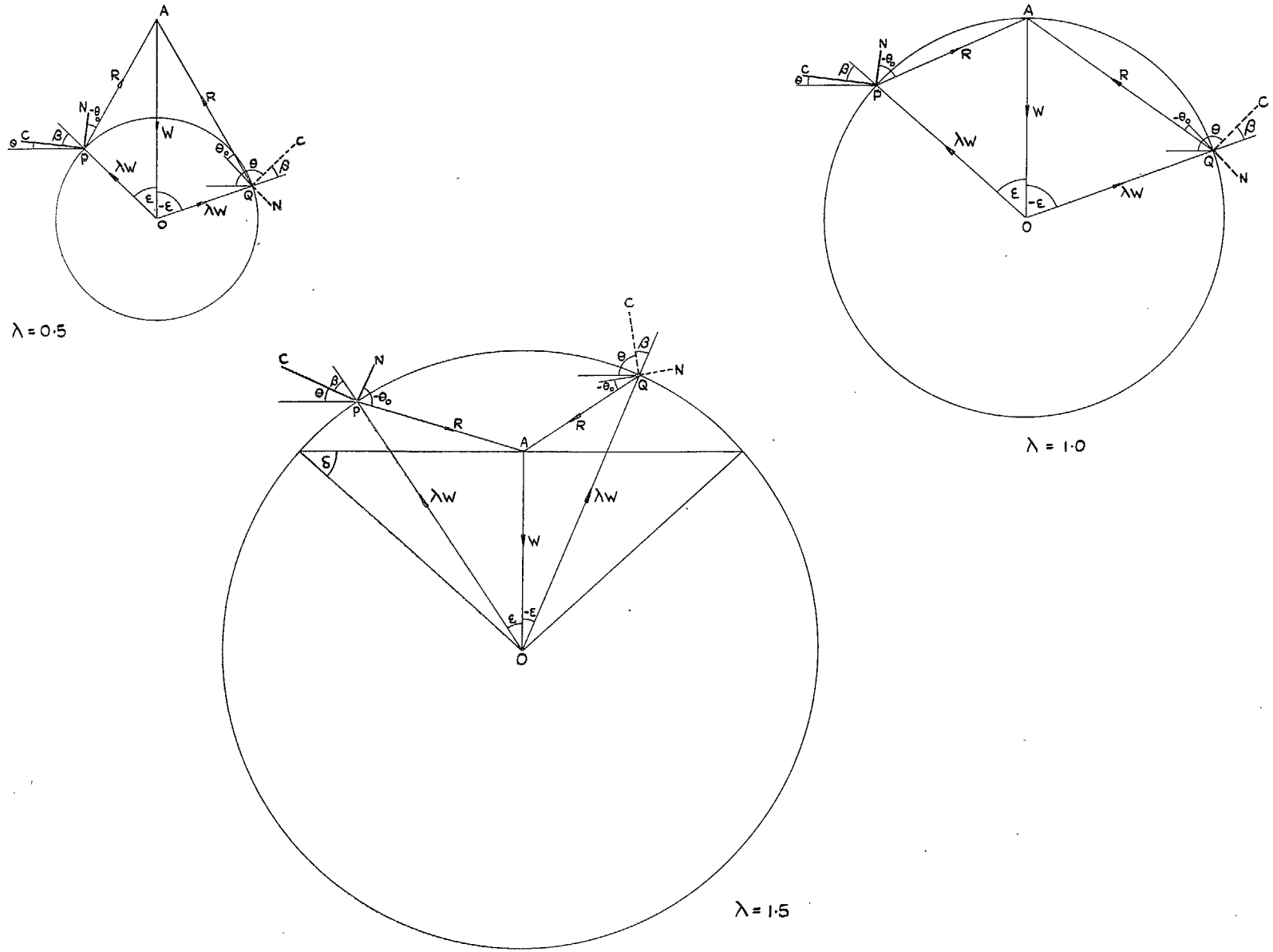

FIG. 8. Principle of graphical construction for attitudes.

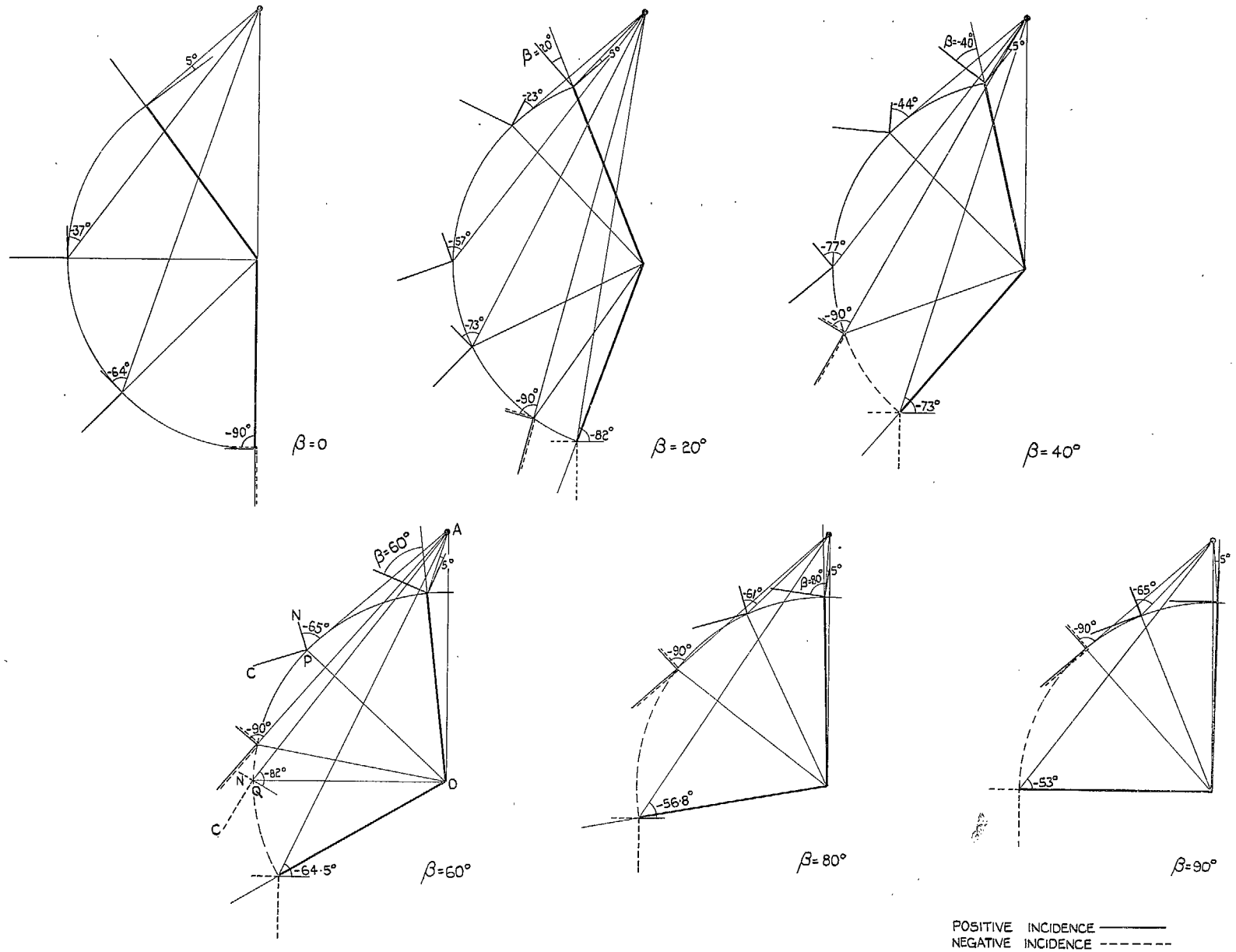

FIG. 9. Attitude sectors for $\lambda = 0{\cdot}75$.
Values of θ_0 are marked on the diagrams.

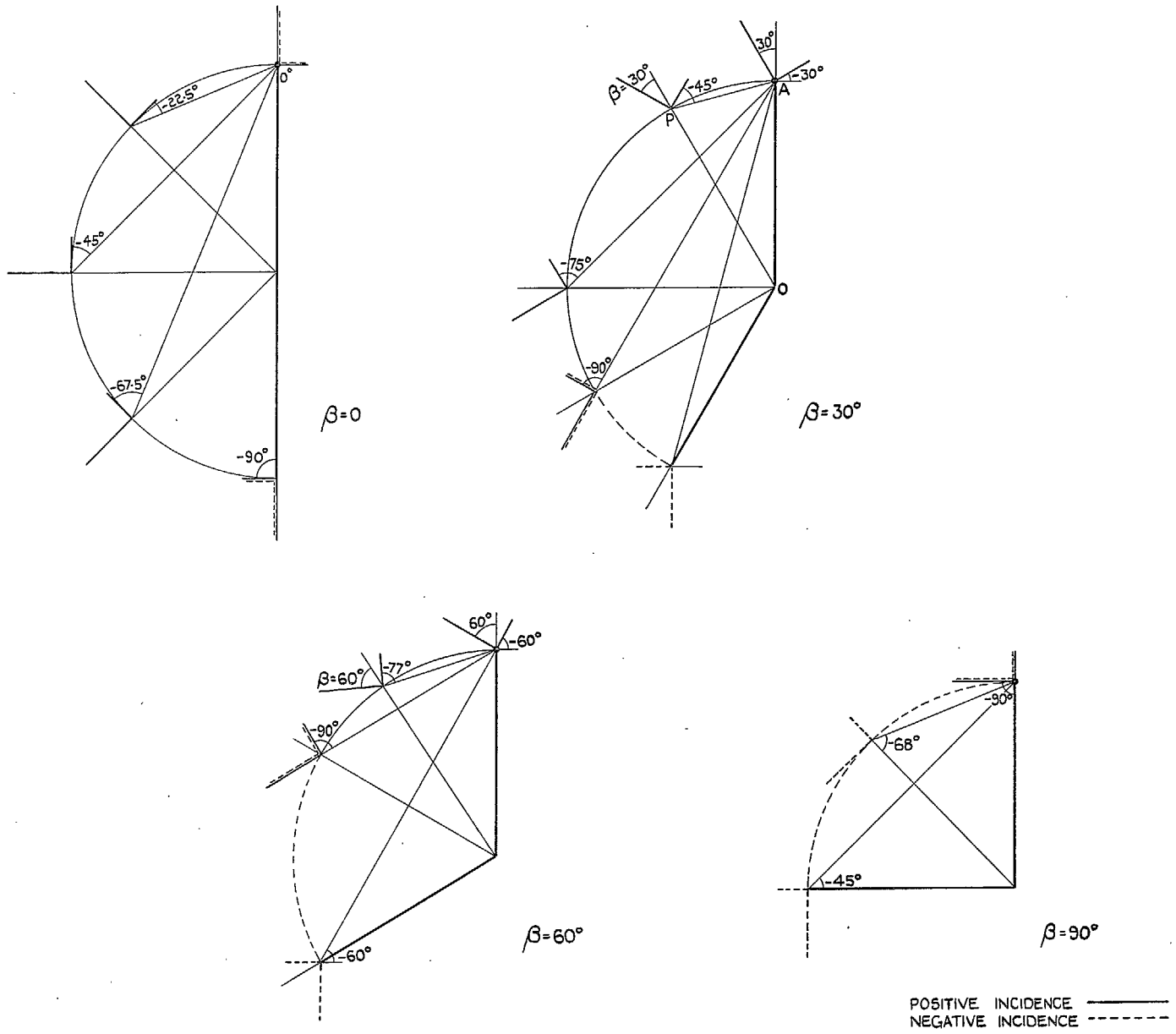

FIG. 10. Attitude sectors for $\lambda = 1{\cdot}0$.
Values of θ_0 are marked on the diagrams.

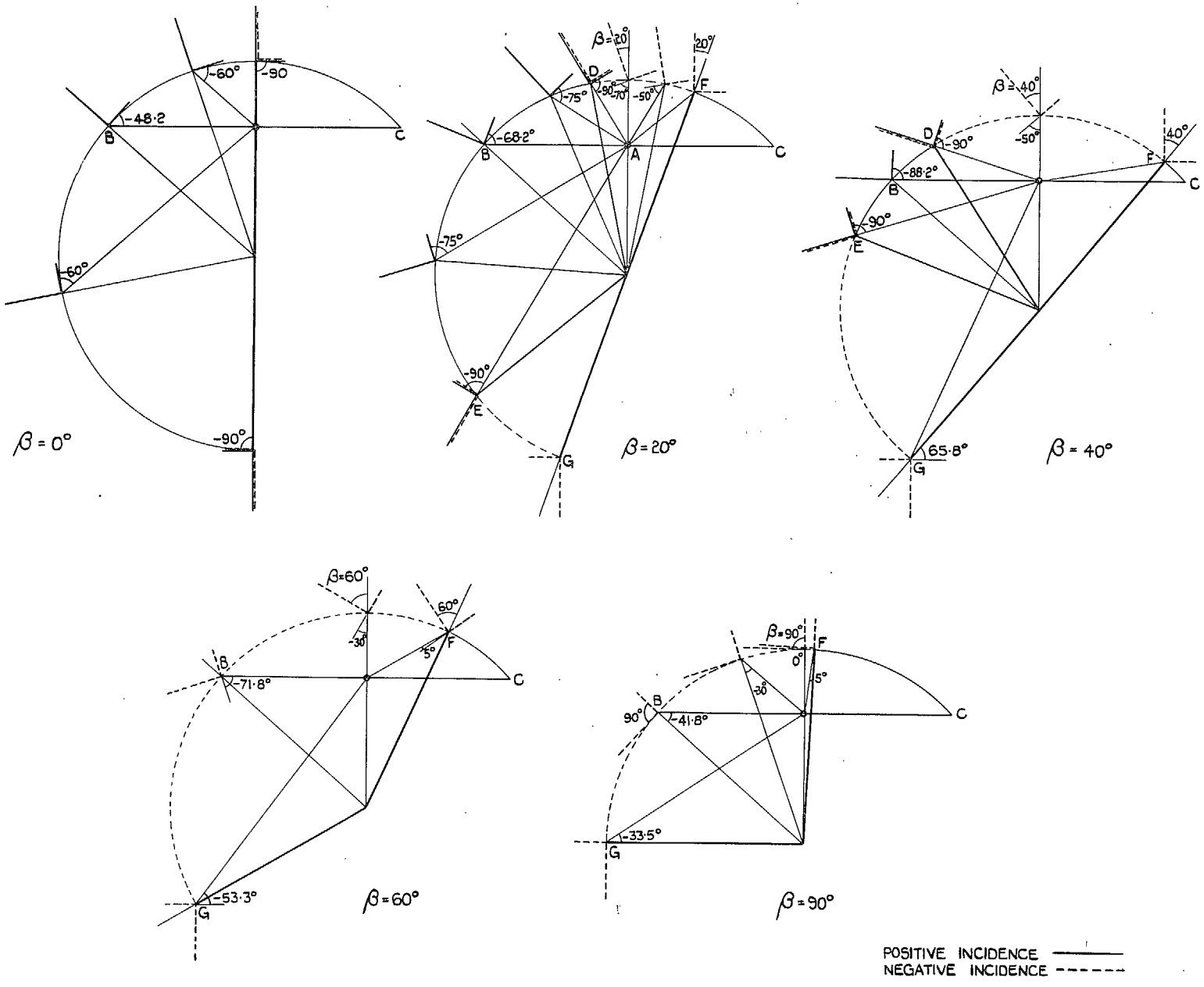

FIG. 11. Attitude sectors for $\lambda = 1{\cdot}5$.
Values of θ_0 are marked on the diagrams.

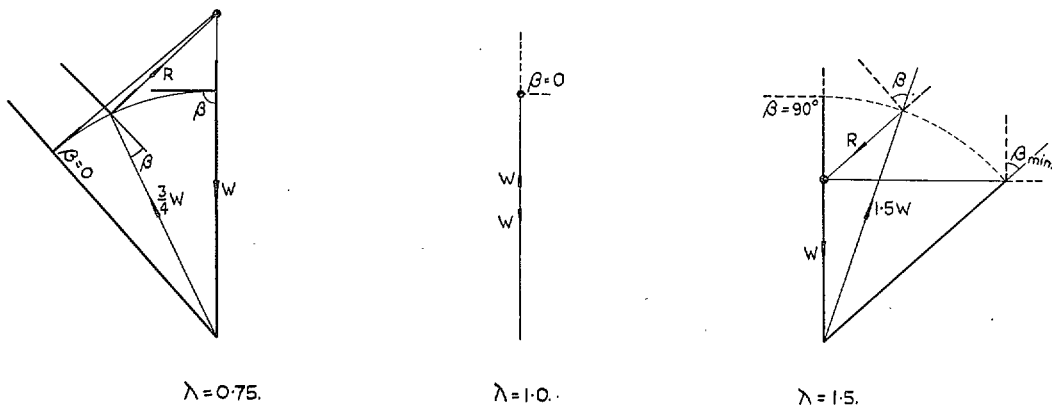

FIG. 12. Attitude sectors for $\theta_0 = 0$, typifying roughly the low-speed regime (*see* FIGS. 13 to 15 for corresponding performance diagrams).

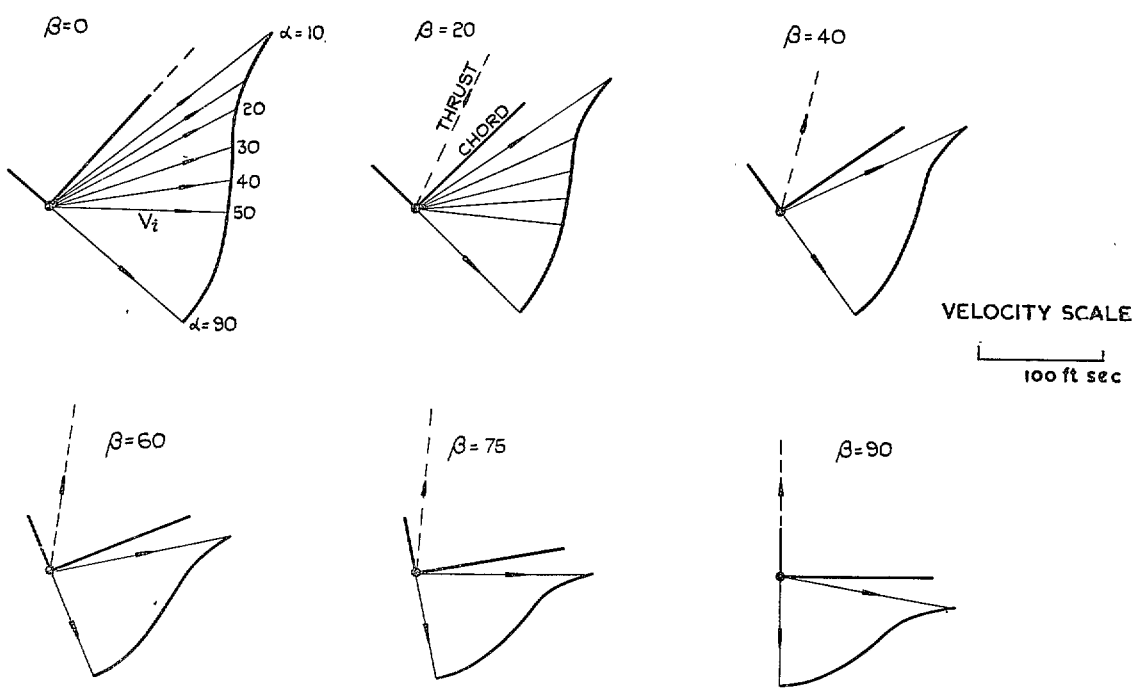

FIG. 13. Approximate performance diagrams for low speed ($\lambda = 0{\cdot}75$, $\theta_0 = 0$, $10 < \alpha < 90$).

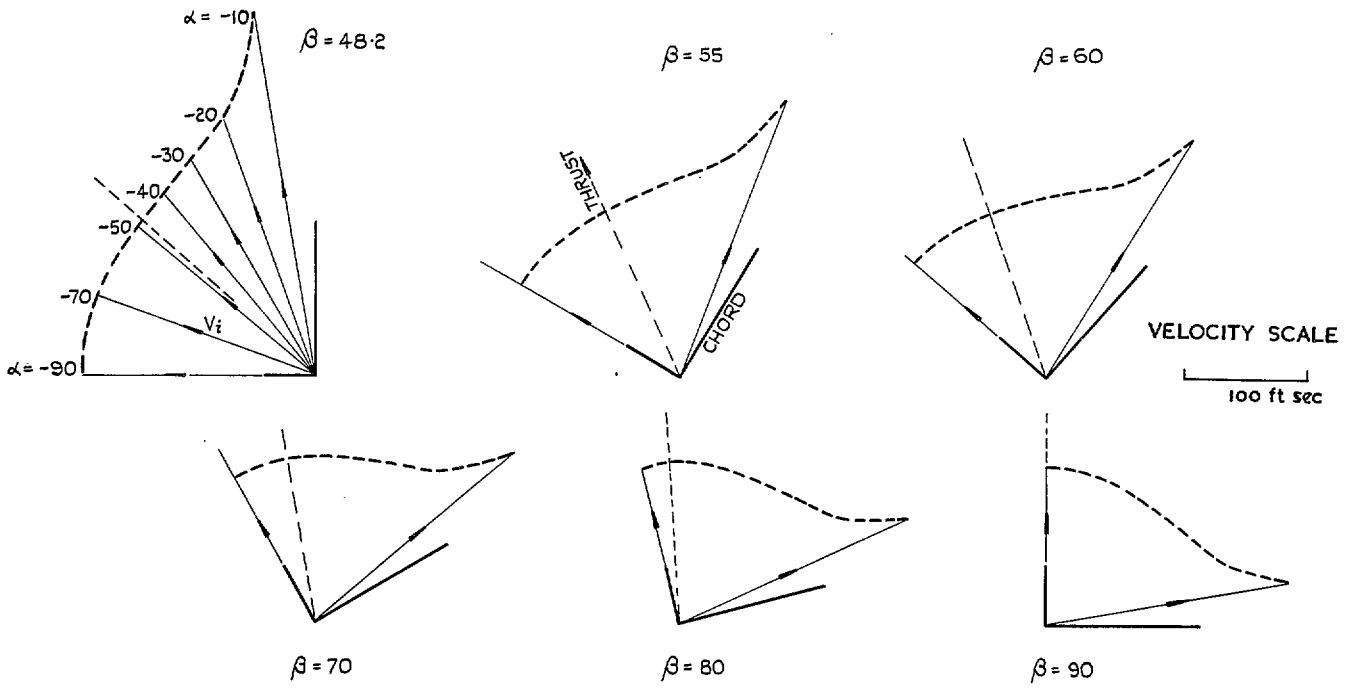

FIG. 14. Approximate performance diagrams for low speed ($\lambda = 1{\cdot}5$, $\theta_0 = 0$, $-10 > \alpha > -90$).

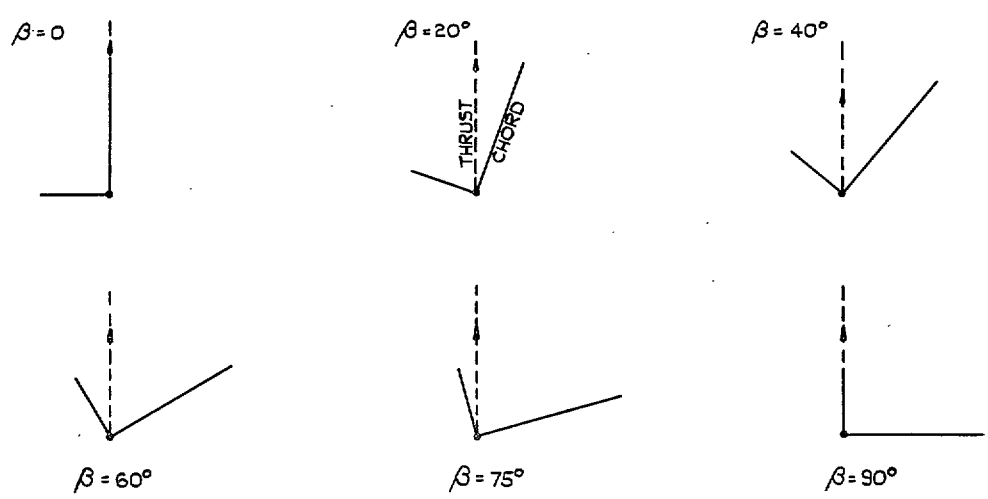

FIG. 15. Stationary positions ($\lambda = 1$).

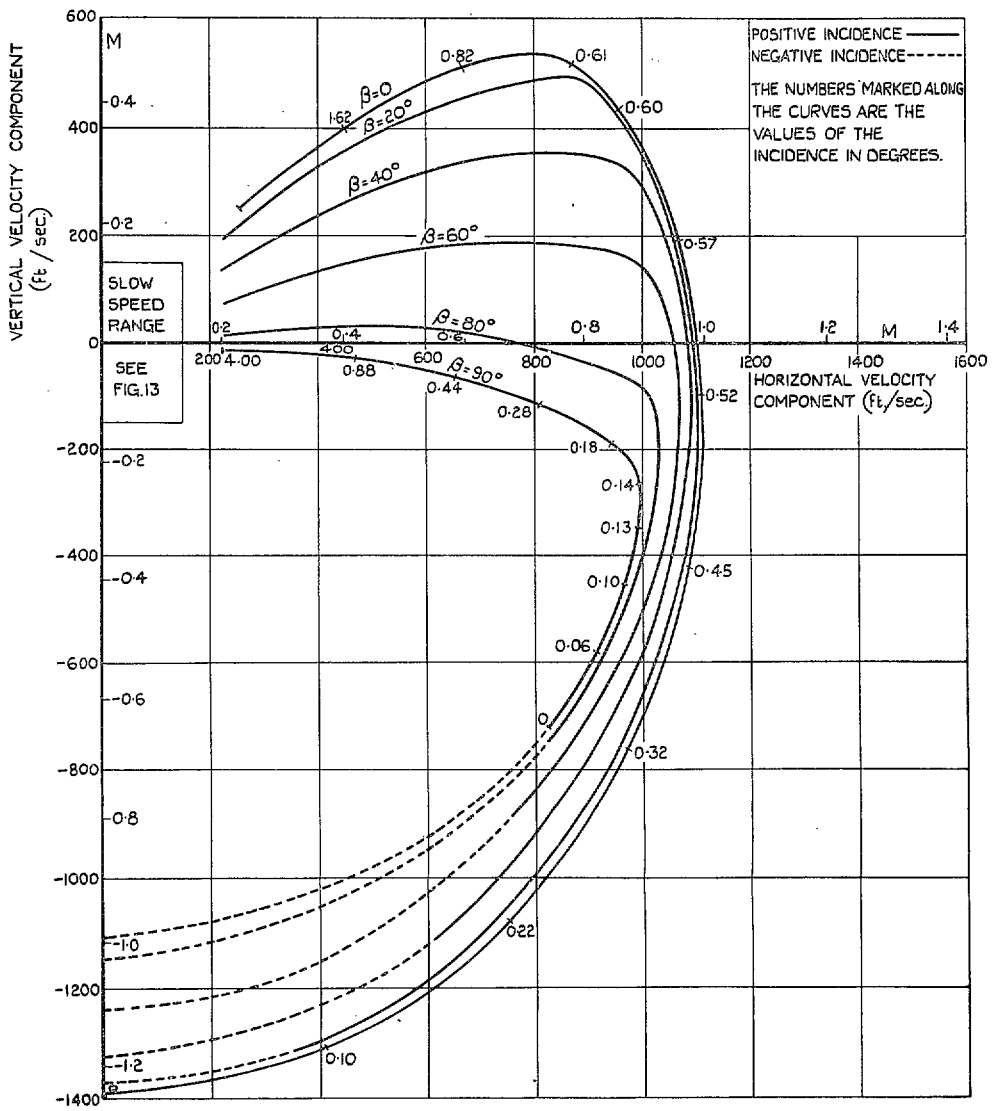

FIG. 16. Velocity vector diagram ($\lambda = 0{\cdot}75$), sea level.

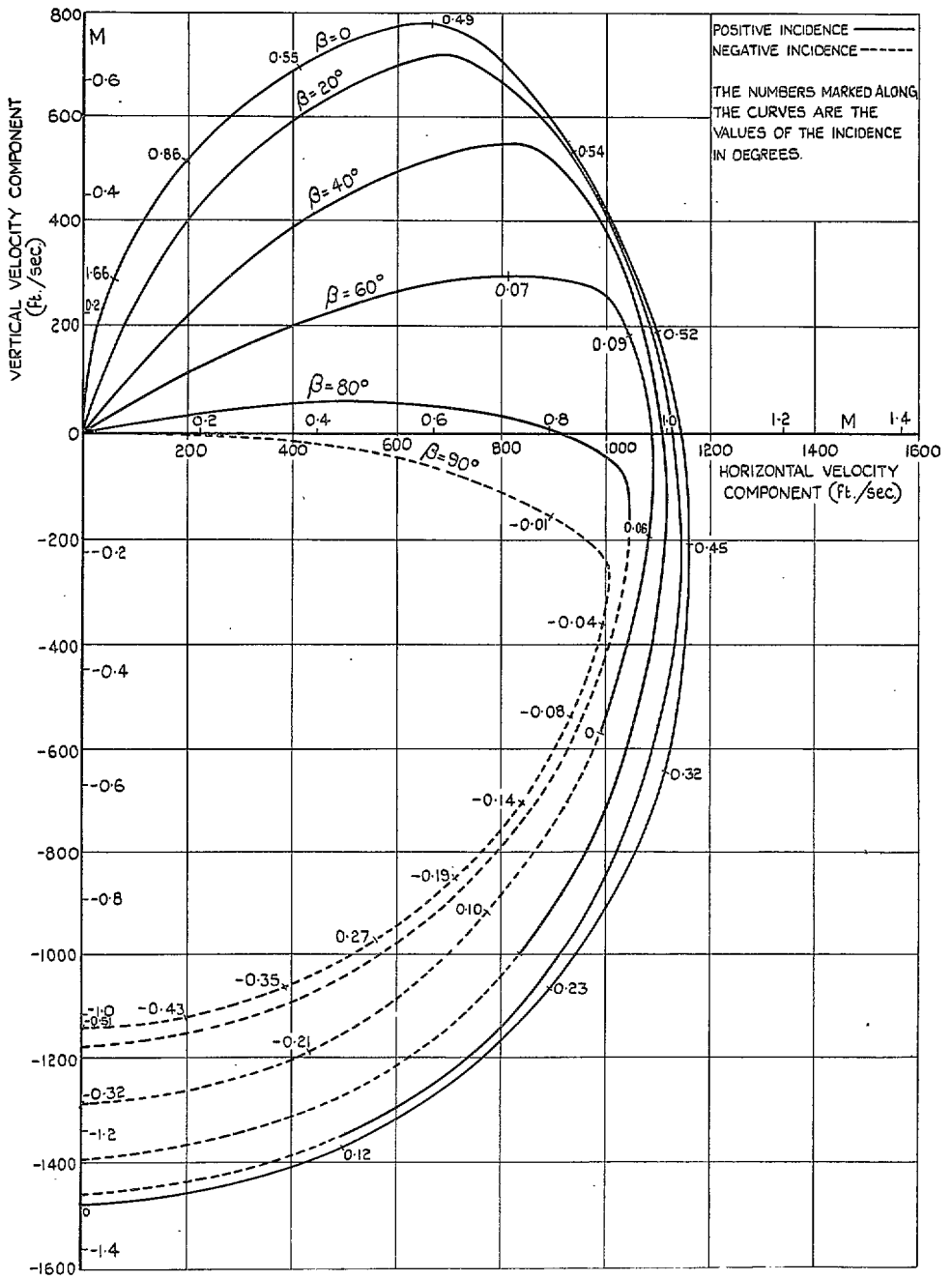

FIG. 17. Velocity vector diagram ($\lambda = 1{\cdot}0$), sea level.

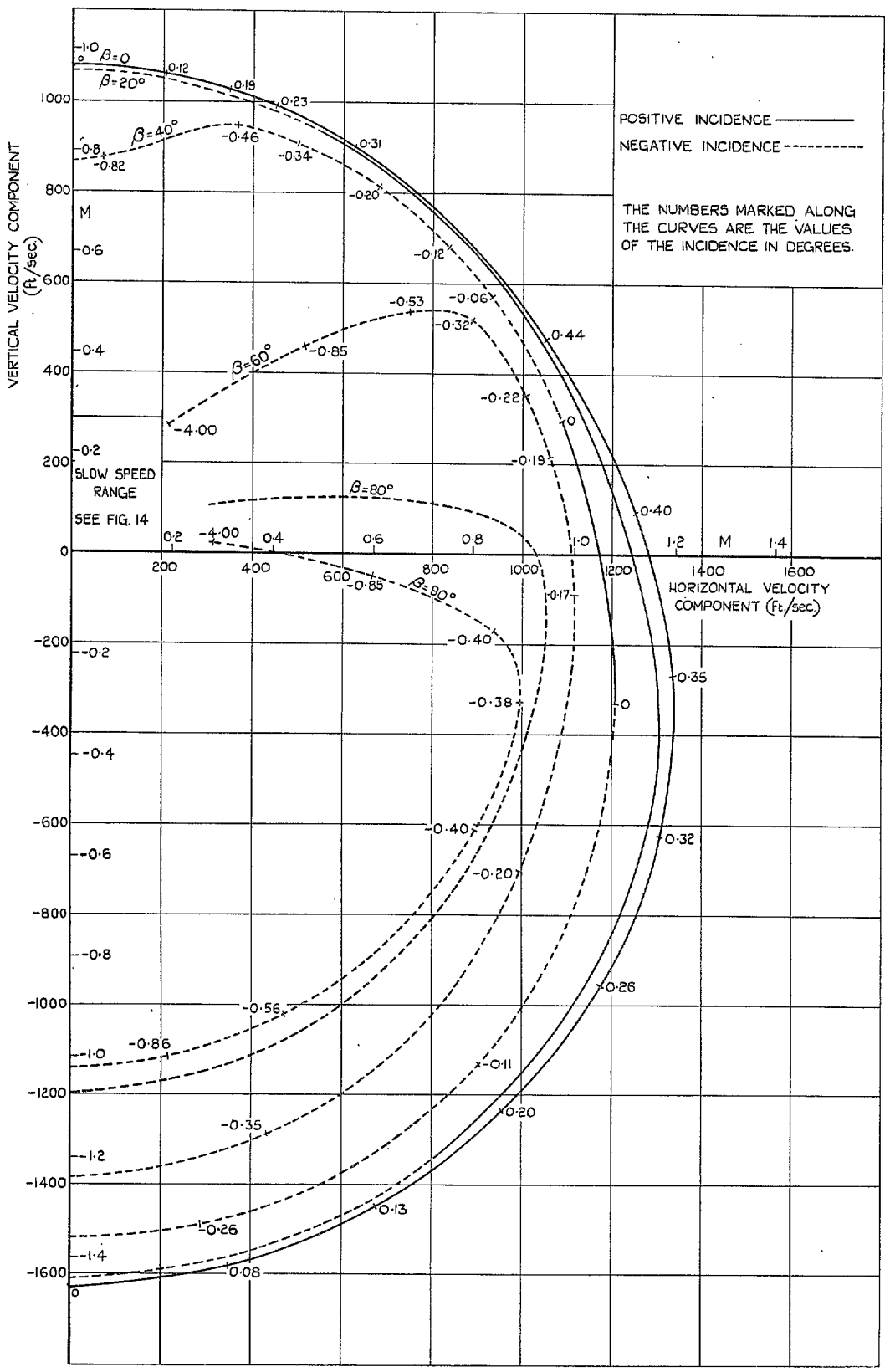

FIG. 18. Velocity vector diagram ($\lambda = 1{\cdot}5$), sea level.

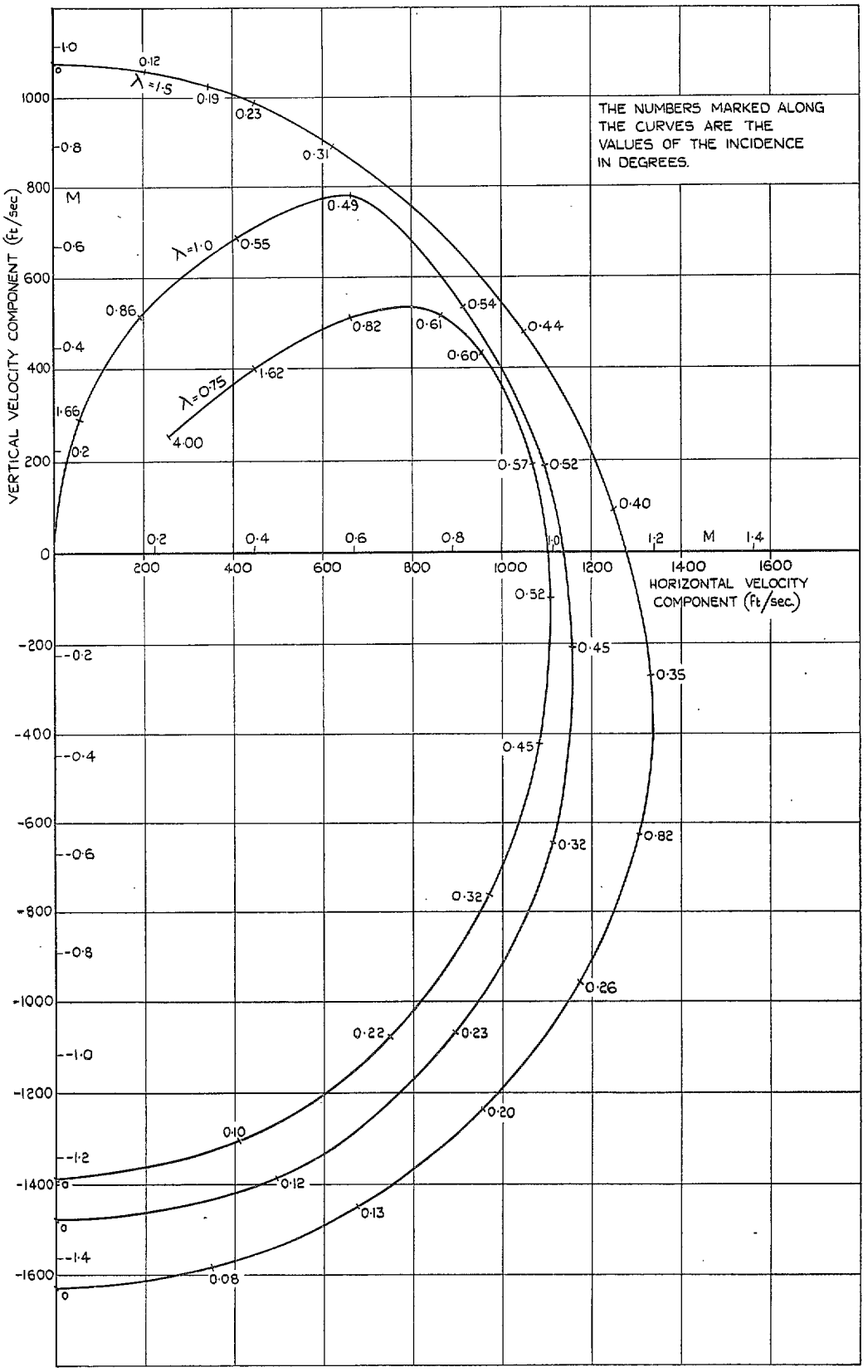

FIG. 19. Velocity vector diagram ($\beta = 0$), sea level.

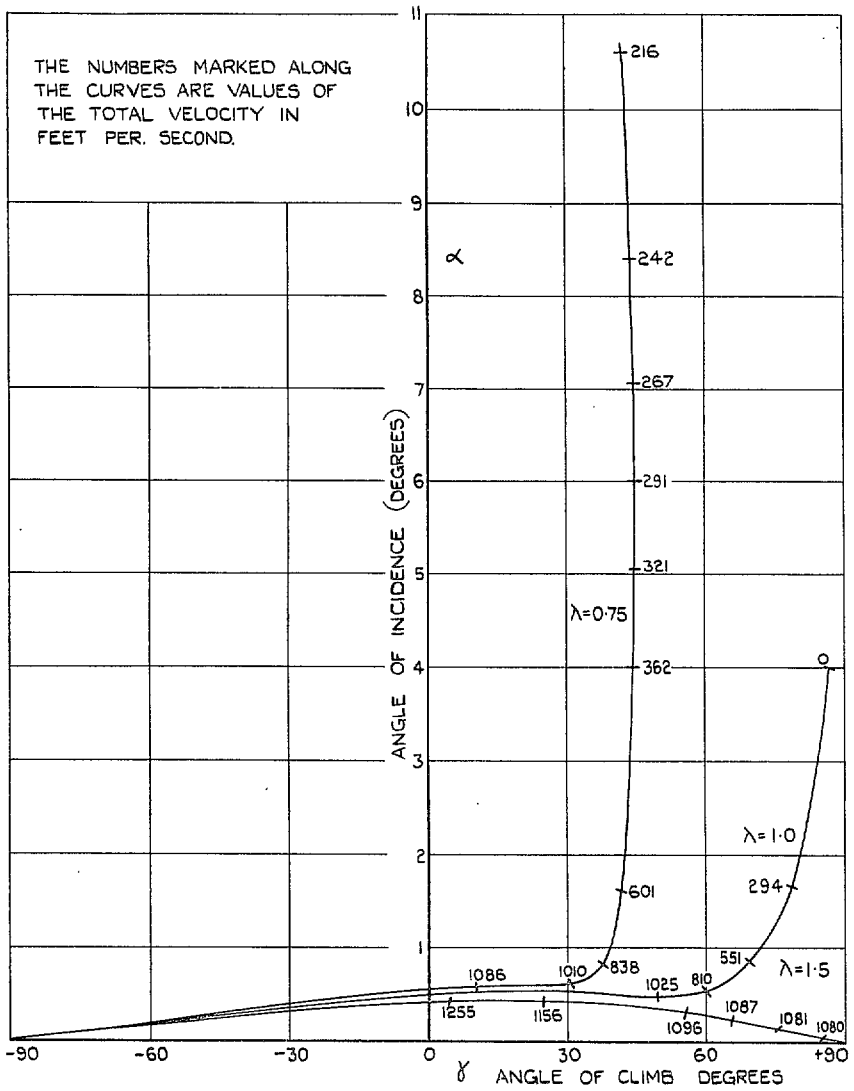

FIG. 20. Relation between incidence and angle of climb ($\beta = 0$).

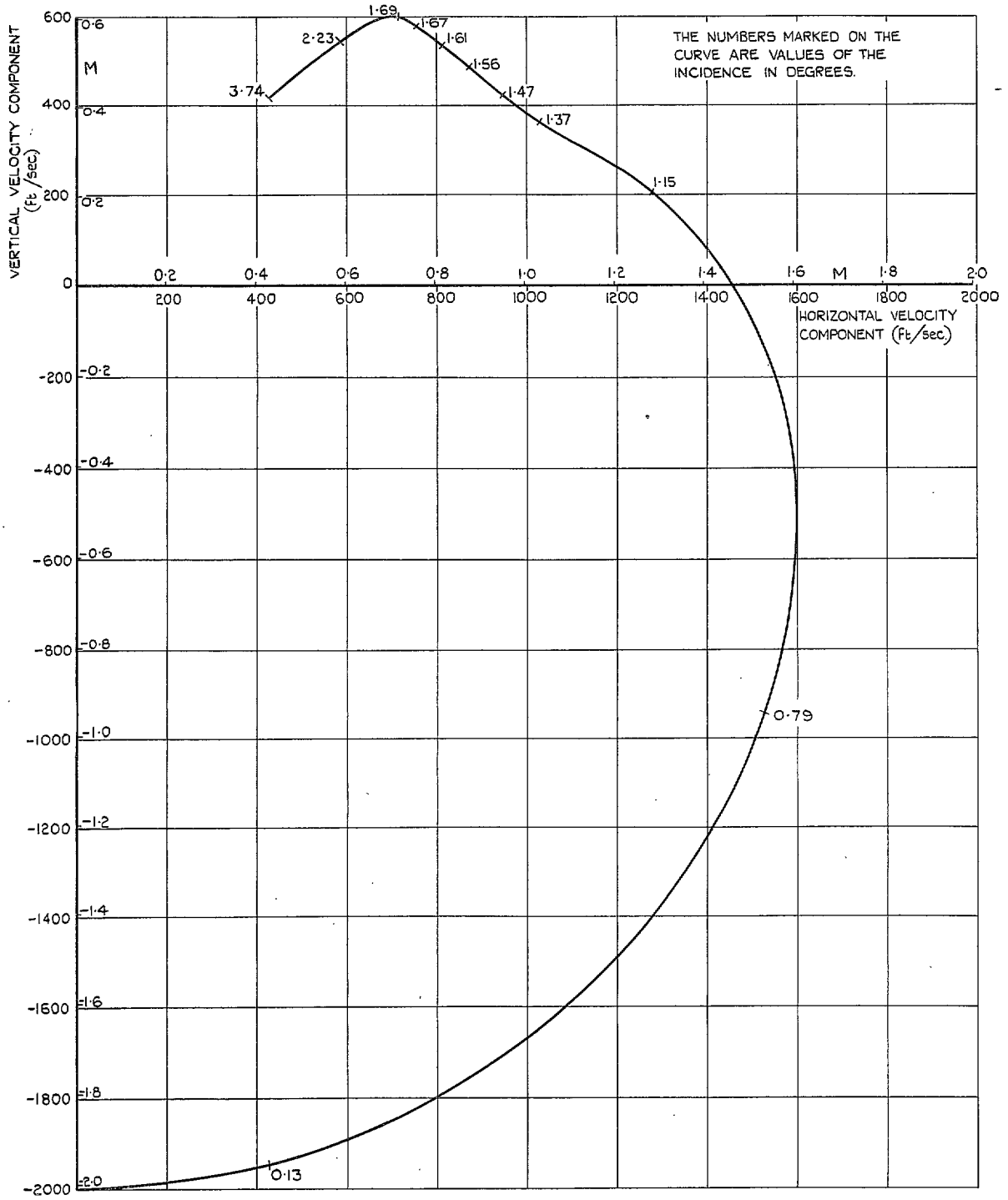

FIG. 21. Velocity vector diagram $\beta = 0$, $\lambda = 0{\cdot}75$ at 30,000 ft, corresponding to $\lambda = 1{\cdot}5$ at sea level.

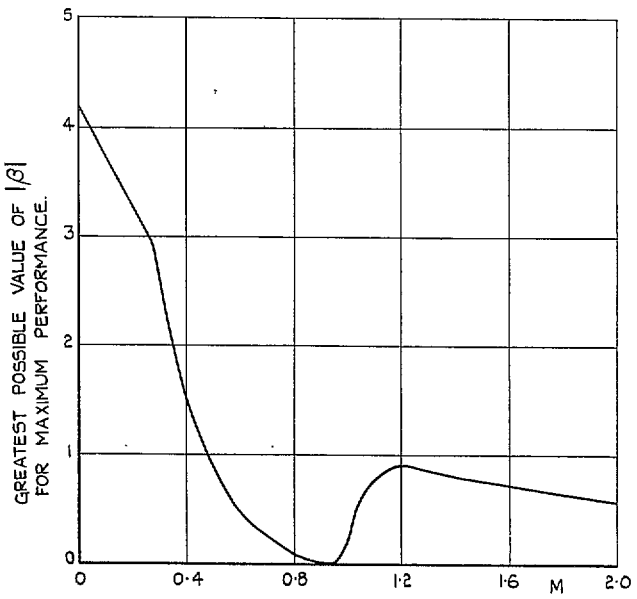

FIG. 22. An upper bound to the value of $|\beta|$ for best performance.

(12471) Wt. 20/680 K.7 6/59 H.P.Co. 34-261 PRINTED IN GREAT BRITAIN

Publications of the Aeronautical Research Council

ANNUAL TECHNICAL REPORTS OF THE AERONAUTICAL RESEARCH COUNCIL (BOUND VOLUMES)—

1939 Vol. I. Aerodynamics General, Performance, Airscrews, Engines. 50*s.* (52*s.*)
Vol. II. Stability and Control, Flutter and Vibration, Instruments, Structures, Seaplanes, etc. 63*s.* (65*s.*)

1940 Aero and Hydrodynamics, Aerofoils, Airscrews, Engines, Flutter, Icing, Stability and Control, Structures, and a miscellaneous section. 50*s.* (52*s.*)

1941 Aero and Hydrodynamics, Aerofoils, Airscrews, Engines, Flutter, Stability and Control, Structures. 63*s.* (65*s.*)

1942 Vol. I. Aero and Hydrodynamics, Aerofoils, Airscrews, Engines. 75*s.* (77*s.*)
Vol. II. Noise, Parachutes, Stability and Control, Structures, Vibration, Wind Tunnels. 47*s.* 6*d.* (49*s.* 6*d.*)

1943 Vol. I. Aerodynamics, Aerofoils, Airscrews. 80*s.* (82*s.*)
Vol. II. Engines, Flutter, Materials, Parachutes, Performance, Stability and Control, Structures. 90*s.* (92*s.* 9*d.*)

1944 Vol. I. Aero and Hydrodynamics, Aerofoils, Aircraft, Airscrews, Controls. 84*s.* (86*s.* 6*d.*)
Vol. II. Flutter and Vibration, Materials, Miscellaneous, Navigation, Parachutes, Performance, Plates and Panels, Stability, Structures, Test Equipment, Wind Tunnels. 84*s.* (86*s.* 6*d.*)

1945 Vol. I. Aero and Hydrodynamics, Aerofoils. 130*s.* (132*s.* 9*d.*)
Vol. II. Aircraft, Airscrews, Controls. 130*s.* (132*s.* 9*d.*)
Vol. III. Flutter and Vibration, Instruments, Miscellaneous, Parachutes, Plates and Panels, Propulsion. 130*s.* (132*s.* 6*d.*)
Vol. IV. Stability, Structures, Wind Tunnels, Wind Tunnel Technique. 130*s.* (132*s.* 6*d.*)

ANNUAL REPORTS OF THE AERONAUTICAL RESEARCH COUNCIL—

1937 2*s.* (2*s.* 2*d.*) 1938 1*s.* 6*d.* (1*s.* 8*d.*) 1939–48 3*s.* (3*s.* 5*d.*)

INDEX TO ALL REPORTS AND MEMORANDA PUBLISHED IN THE ANNUAL TECHNICAL REPORTS, AND SEPARATELY—

April, 1950 . . . . . R. & M. No. 2600 2*s.* 6*d.* (2*s.* 10*d.*)

AUTHOR INDEX TO ALL REPORTS AND MEMORANDA OF THE AERONAUTICAL RESEARCH COUNCIL—

1909–January, 1954 . . . R. & M. No. 2570 15*s.* (15*s.* 8*d.*)

INDEXES TO THE TECHNICAL REPORTS OF THE AERONAUTICAL RESEARCH COUNCIL—

December 1, 1936 — June 30, 1939	R. & M. No. 1850	1*s.* 3*d.* (1*s.* 5*d.*)
July 1, 1939 — June 30, 1945	R. & M. No. 1950	1*s.* (1*s.* 2*d.*)
July 1, 1945 — June 30, 1946	R. & M. No. 2050	1*s.* (1*s.* 2*d.*)
July 1, 1946 — December 31, 1946	R. & M. No. 2150	1*s.* 3*d.* (1*s.* 5*d.*)
January 1, 1947 — June 30, 1947	R. & M. No. 2250	1*s.* 3*d.* (1*s.* 5*d.*)

PUBLISHED REPORTS AND MEMORANDA OF THE AERONAUTICAL RESEARCH COUNCIL—

Between Nos. 2251–2349	R. & M. No. 2350	1*s.* 9*d.* (1*s.* 11*d.*)
Between Nos. 2351–2449	R. & M. No. 2450	2*s.* (2*s.* 2*d.*)
Between Nos. 2451–2549	R. & M. No. 2550	2*s.* 6*d.* (2*s.* 10*d.*)
Between Nos. 2551–2649	R. & M. No. 2650	2*s.* 6*d.* (2*s.* 10*d.*)
Between Nos. 2651–2749	R. & M. No. 2750	2*s.* 6*d.* (2*s.* 10*d.*)

Prices in brackets include postage

HER MAJESTY'S STATIONERY OFFICE

York House, Kingsway, London, W.C.2; 423 Oxford Street, London, W.1; 13a Castle Street, Edinburgh 2; 39 King Street, Manchester 2; 2 Edmund Street, Birmingham 3; 109 St. Mary Street, Cardiff; Tower Lane, Bristol 1; 80 Chichester Street, Belfast *or through any bookseller.*

S.O. Code No. 23–3096